PAPER

Check for updates

Formation of oxygen vacancies in Li$_2$FeSiO$_4$: first-principles calculations

Lihong Zhang,[a] Shunqing Wu, [ID][a] Jianwei Shuai, [ID][a] Zhufeng Hou [ID] *[b] and Zizhong Zhu [ID] *[ac]

The formation of oxygen vacancies could affect various properties of oxides. Herein we have investigated the formation energies of an oxygen vacancy (V$_O$) with the relevant charge states in bulk *Pnma*-Li$_2$FeSiO$_4$ using first-principles calculations. The formation energies of the V$_O$ are essentially dependent on the atomic chemical potentials that represent the experimental conditions. The calculated formation energies of an oxygen vacancy in different charge states indicate that it would be energetically favorable to fully ionize the oxygen vacancy in Li$_2$FeSiO$_4$. The presence of V$_O$ is accompanied by a distinct redistribution of the electronic charge densities only around the Fe and Si ions next to the O-vacancy site, which shows a very local influence on the host material arising from V$_O$. This local characteristic is also confirmed by the calculated partial densities of states (PDOS). We also studied the influence of substitutional (Mn$_{Fe}$ and Co$_{Fe}$) and cation vacancy defects (*i.e.*, V$_{Fe}$ and V$_{Li}$) in the vicinity of an O-vacancy on the formation of an O-vacancy, respectively. We find that the calculated interaction energies between these defects and the oxygen vacancy are all negative, which implies that the formation of an oxygen vacancy becomes easier when the above defects are introduced. Compared to the substitutional defects, the interaction energies between the vacancy defects and the oxygen vacancy are significantly larger. Among them, the interaction energy between V$_{Fe}$ and V$_O$ is the largest.

1. Introduction

The cathode materials of Li-ion batteries (LIBs) are considered to be one of the major factors in determining the electrochemical performance of the batteries.[1,2] The current main commercialized cathode materials, such as layered oxide LiCoO$_2$, spinel LiMn$_2$O$_4$, and polyanionic compound LiFePO$_4$ have been intensively studied over the past few decades.[1–8] Since the Li-rich transition-metal (TM) oxide Li$_2$FeSiO$_4$ was first reported by Nytén *et al.*,[9] it has been considered as a promising cathode candidate for rechargeable LIBs because of its outstanding characteristics, such as low cost, high potential capacity, and abundant resources.[10–13] Unfortunately, Li$_2$FeSiO$_4$ exhibits poor electronic conductivity and a low lithium-ion diffusion rate, which restrict its practical applications in new electric devices. Therefore, various strategies have been introduced to improve the aforementioned limitations of Li$_2$FeSiO$_4$, such as carbon-coating, particle size reducing and elemental

doping.[14–23] Among these optimization approaches, chemical doping, which includes cationic and anionic doping, has been attracting more attention.[24,25] In defect chemistry, the introduction of oxygen vacancies in oxides is typically a "native defect". Therefore, the understanding of the behavior of oxygen vacancies in host oxides becomes very important and could help lay the foundation for anion defect engineering to boost the electrochemical performance of cathode materials.

The formation of oxygen vacancies could affect various properties of the host oxide materials, such as the cycling stability in the battery system.[26–30] Recently, Bruce *et al.* reported that the formation of oxygen vacancies was not correlated with the O redox in the battery material P2-Na$_{0.67}$Mg$_{0.28}$Mn$_{0.72}$O$_2$, and they also proposed the reasons for the formation of oxygen vacancies.[31] The oxygen loss was attributed to the absence of a local coordinated cation around the oxygen, which left the oxygen severely under-bonded and triggered the oxygen loss.[31] However, there were few studies on oxygen vacancy formations in Li$_2$FeSiO$_4$ cathode materials.[29] In order to better improve the performances of Li$_2$FeSiO$_4$ as a cathode of LIBs and its structural cycling stability, it is essential to study the oxygen vacancy formation in the material.

In this work, first-principles calculations are performed to study the formation of oxygen vacancy (V$_O$) in bulk *Pnma*-Li$_2$FeSiO$_4$. The calculation results reveal clear trends of the

[a] *Department of Physics, Xiamen University, Xiamen 361005, China*

[b] *State Key Laboratory of Structural Chemistry, Fujian Institute of Research on the Structure of Matter, Chinese Academy of Sciences, Fuzhou 350002, China. E-mail: houzhufeng@fjirsm.ac.cn*

[c] *Fujian Provincial Key Laboratory of Theoretical and Computational Chemistry, Xiamen University, Xiamen 361005, China. E-mail: zzhu@xmu.edu.cn*

formation energies of V_O depending on the temperature, the oxygen partial pressure and the Fermi level. The increased temperature, decreased oxygen partial pressure and Fermi level decrease the formation energy of the oxygen vacancy. Meanwhile, we further investigated the effects resulting from the introduction of one oxygen vacancy by calculating the charge densities and electronic density of states. We also studied the influences on the formation of an O-vacancy by the substitutional and vacancy defects in the vicinity of the O-vacancy, respectively. Our work can help in understanding the factors controlling V_O formation.

2. Details of computational methods

Our calculations on Li_2FeSiO_4 were performed using the Vienna *ab initio* simulation package (VASP), which is based on the density functional theory (DFT),[32,33] the plane wave basis, and the projector augmented wave (PAW) representation.[34] The exchange–correlation energy functional was treated within the spin–polarized generalized gradient approximation (GGA) and was parameterized using the Perdew–Burke–Ernzerhof formula (PBE).[35] Wave functions were expanded up to a cutoff of 550 eV of the plane-wave kinetic energy. Brillouin-zone integration was performed within the Monkhorst–Pack scheme,[36] in which the regular Γ-centered $3 \times 5 \times 6$ and $1 \times 2 \times 2$ **k**-point meshes were used for the employed primitive unit cell and $2 \times 2 \times 2$ supercell of Li_2FeSiO_4, respectively. The convergence criterion in the self-consistent field (SCF) calculations was set to 10^{-5} eV for the total energy. In the geometry optimization all atoms were allowed to relax until the maximal residual Hellmann–Feynman forces on the atoms were smaller than 0.02 eV Å^{-1}. To take into account the on-site Coulombic interaction of Fe 3d electrons in Li_2FeSiO_4, we employed the GGA+U approach of Dudarev *et al.*[37] The effective interaction $U_{eff} = U - J$ of 4 eV was used for Fe 3d electrons. For the Mn and Co doped cases, the U_{eff} values for Mn and Co 3d electrons were both set to 5 eV. Herein we focused on the ferromagnetic configuration of Li_2FeSiO_4 because it is energetically more favorable.

3. Results and discussions

3.1 Formation energies of oxygen vacancies

The formation energy of an oxygen vacancy plays a crucial role in determining the properties of a material. The calculated oxygen vacancy formation energies can be used to characterize the probability of O vacancy generation in a material. The oxygen vacancy formation energy in charge state q, $E_f(O^q)$, can be defined according to the following equation:[38,39]

$$E_f(O^q) = E(O^q) - E(0) + \Delta n \mu_O + q(E_{VBM} + \varepsilon_F) + E_{corr}, \quad (1)$$

where the $E(O^q)$ and $E(0)$ are the calculated total energies of the supercell containing an oxygen vacancy in charge state q and of the supercell of the perfect material, respectively. Δn indicates the number of oxygen atoms which has been removed from ($\Delta n < 0$) or added to ($\Delta n > 0$) the perfect supercell in forming the oxygen vacancies. μ_O is the chemical potential of an O atom,

representing the energy of the reservoir with which the removed/added O atoms are exchanged. ε_F is the Fermi level or electronic chemical potential relative to the valence band maximum (VBM) in the perfect crystal (E_{VBM}). We allow ε_F to vary from 0 to E_g, where E_g is the fundamental band gap obtained from the perfect bulk material. The E_{corr} is a correction term to account for the image-charge and potential alignment corrections for the charged defect since a neutralizing background was applied to the supercell in the calculation of a charged defect. We have employed the approach proposed by Kumagai and Oba[40] to calculate the E_{corr} for oxygen vacancies in charged states in Li_2FeSiO_4.

The atomic chemical potential μ_O in eqn (1) is a variate representing the experimental condition. The thermodynamic expression of the oxygen chemical potential $\mu_O(T, P)$ with respect to temperature T and pressure P for the gas-phase oxygen (O_2) is as follows:[41]

$$\mu_O(T, P) = \mu_O(T_0, P_0) + \delta\mu_O(T, P_1) + \frac{1}{2}k_B T \ln\left(\frac{P}{P_1}\right) \quad (2)$$

where $\mu_O(T_0, P_0)$ is the oxygen chemical potential at zero Kelvin ($T_0 = 0$ K, $P_0 = 0$ atm) and standard atmospheric pressure ($P_1 = 1$ atm), which was approximated to half of the total energy of an isolated O_2 molecule obtained by DFT calculations, $\frac{1}{2}E(O_2)$, together with a correction of -1.36 eV because the DFT typically overestimated the cohesive energy of an isolated O_2 molecule.[42] P is the partial pressure of O_2 gas. k_B is the Boltzmann's constant. $\delta\mu_O(T, P_1)$ denotes the contribution of the temperature to the oxygen chemical potential at the particular pressure P_1, which is taken from ref. 43.

We have previously studied the structures and electronic properties of several polymorphs of X_2MSiO_4 (X = Li, Na; M = Mn, Fe, Co)[44] with space groups of *Cmcm, Pmna*, and $P2_12_12_1$. These structures of Li_2FeSiO_4 are all mechanically, dynamically, and thermodynamically stable.[45] For these different polymorphs of Li_2FeSiO_4, they actually possess very similar redox reaction mechanisms.[45] Thus, herein we pay attention to only the prototype structure of *Pnma*-Li_2FeSiO_4, which has the lowest cohesive energy among the three polymorphs, as shown in Fig. 1(a). The primitive unit cell of *Pnma*-Li_2FeSiO_4 contains $4 \times Li_2FeSiO_4$ formula units (f.u.) and the structure is generated from tetrahedral networks. All the cations of Li^+, Fe^{2+} and Si^{4+} in this structure occupy the center of tetrahedra. For the coordinated oxygen atoms, each O is assigned to two Li atoms, one Fe atom and one Si atom. Half of the tetrahedra point along the c-axis and the other half point along the opposite direction of the c-axis, respectively. Otherwise, Li ions line up in channels along the b-axis and LiO_4 tetrahedra share an edge with each other. Firstly, we optimized the primitive unit cell of *Pnma*-Li_2FeSiO_4. The calculated lattice parameters are $a = 10.77$, $b = 6.32$, and $c = 5.04$ Å, in good agreement with the previous results.[44] The calculated average bond lengths of Li–O, Fe–O, and Si–O are 1.98, 2.04, and 1.66 Å, respectively, which are the same as those reported in ref. 45. There are three non-equivalent sites for oxygen in the bulk *Pnma*-Li_2FeSiO_4, which

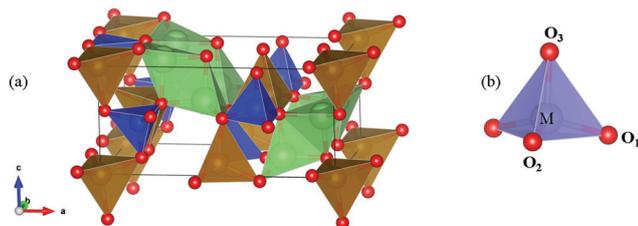This journal is © the Owner Societies 2021

Phys. Chem. Chem. Phys., 2021, **23**, 20444–20452 | **20445**

Fig. 1 (a) Crystal structure of *Pnma*-Li$_2$FeSiO$_4$. LiO$_4$, FeO$_4$, and SiO$_4$ tetrahedra are colored in light green, light brown and light blue, respectively. Oxygen atoms are denoted by red balls. (b) Light purple tetrahedron is the schematic representation of the MO$_4$ tetrahedra with M = Li, Fe or Si. The non-equivalent coordinated oxygen atoms are denoted as O1, O2 and O3, respectively.

are denoted as O1, O2, and O3, as illustrated in Fig. 1(b). Therefore, by removal of the corresponding O1, O2, or O3 atom, three configurations of oxygen vacancies (*i.e.*, V$_{O1}$, V$_{O2}$, and V$_{O3}$) were considered in our calculations. To simulate the single oxygen vacancy in Li$_2$FeSiO$_4$ and to avoid the interaction between oxygen vacancy and its periodic images, we employed a 2 × 2 × 2 supercell, whose perfect case contains 256 atoms (*i.e.*, 32 × Li$_2$FeSiO$_4$ f.u.), and the corresponding concentration of oxygen vacancy is about 0.78%.

Fig. 2 shows the partial density of states (PDOS) of Fe-3d, Si-3s, 3p and O-2p orbitals for the perfect bulk *Pnma*-Li$_2$FeSiO$_4$. Clearly, Li$_2$FeSiO$_4$ is a semiconductor and its band gap is about 2.90 eV as predicted by the present GGA+U calculations. Both the electronic states at the VBM and the conduction-band minimum (CBM) are mainly composed of Fe 3d orbitals. The atomic energy level of Si 3p orbitals is slightly deeper than that of Fe 3d orbitals. As mentioned above, the averaged Si–O bond length is much shorter than the averaged Fe–O bond length. The bonding states arising from the hybridization between the Si 3p orbitals and the O 2p orbitals appear in lower energy range (*i.e.*, about −6 to −2 eV below the VBM) in the valence bands, while the antibonding counterpart is much above the
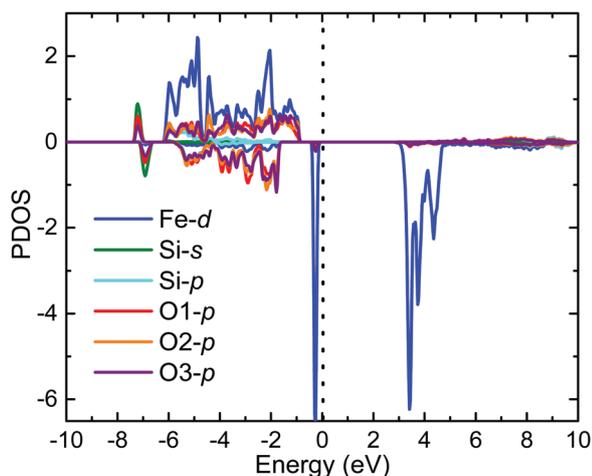
CBM. As for the tetrahedral configuration of Fe, the Fe 3d orbitals split into the t$_{2g}$ (d$_{xy}$, d$_{xz}$, and d$_{yz}$) and e$_g$ (d$_{x^2−y^2}$ and d$_{z^2}$) orbitals. The Fe 3d-t$_{2g}$ orbitals are hybridized strongly with the O 2p orbitals. The bonding states due to the hybridization between the Fe 3d-t$_{2g}$ and O 2p orbitals appear in the range from −6 eV to −1 eV for the majority spin (and −7 eV to −2 eV for the minority spin) below the VBM. The sharp states near the VBM for the minority spin dominantly come from the nearly non-bonding Fe 3d-e$_g$ orbitals, while robust states near the CBM (minority spin) are mainly contributed by the antibonding states of the hybridized Fe 3d-t$_{2g}$ and O 2p orbitals.

We first discuss the formation energy of oxygen vacancies. We investigate here all three non-equivalent oxygen vacancies at their three possible charge states (*i.e.*, q = 0, +1 and +2) labeled V$_O^0$, V$_O^{1+}$ and V$_O^{2+}$. For a single oxygen vacancy, the relative energy difference in between the non-equivalent oxygen vacancies is independent of the oxygen chemical potential. So, we focus on the oxygen-rich case (*i.e.*, T = 0 and P = P^0 = 1 atm in eqn (2)) to simplify the presentation. The calculated formation energies for non-equivalent O vacancies at different charge states in *Pnma*-Li$_2$FeSiO$_4$ are shown in Fig. 3 as a function of the Fermi energy, which is given with respect to the VBM (*i.e.*, VBM corresponds to ε_F = 0 and CBM to ε_F = E_g). The formation energies of oxygen vacancies at ε_F = 0 and ε_F = E_g are also summarized in Table 1. We can see that the oxygen vacancy at the O3 site (*i.e.*, V$_{O3}$) is the most stable in the cases of q = 0 and +1, while the oxygen vacancy becomes slightly less unstable at the O2 site (*i.e.*, V$_{O2}$) in the case of q = +2. We should point out that the relative energy difference between V$_{O3}^{2+}$ and V$_{O2}^{2+}$ is less than 5 meV per cell. In a wide range of ε_F, the charge state of q = +2 for all three non-equivalent oxygen vacancies is energetically more favorable. In fact, there are very small relative energy differences among the three different types of oxygen vacancies at the same charged state, in view of the similar coordination environments of the three kinds of O-sites (see Fig. 1). In the following sections, we consider only the
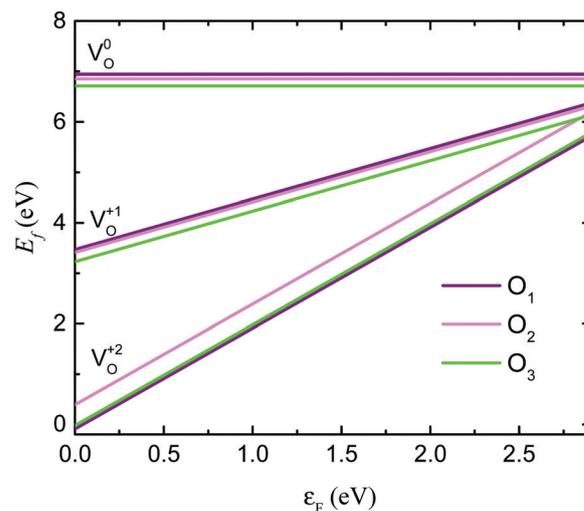

Fig. 2 Atomic decomposed partial densities of states (PDOS) for perfect *Pnma*-Li$_2$FeSiO$_4$. The Fermi level is set to 0 eV, as marked by the dotted line.

Fig. 3 Formation energies of non-equivalent O vacancies at the different charge states in bulk *Pnma*-Li$_2$FeSiO$_4$ as a function of Fermi energy.

Table 1 The calculated formation energies of non-equivalent O vacancies at the different charge states in the bulk *Pnma*-Li$_2$FeSiO$_4$, at $\varepsilon_F = 0$ and $\varepsilon_F = E_g$

Charge states	O-vacancy formation energies (eV)					
	$\varepsilon_F = 0$			$\varepsilon_F = E_g$		
	O1	O2	O3	O1	O2	O3
V_O^0	6.94	6.85	6.71	6.94	6.85	6.71
V_O^{1+}	3.47	3.41	3.23	6.38	6.31	6.14
V_O^{2+}	−0.09	0.39	−0.02	5.72	6.20	5.79

V_{O3}, which has the lowest formation energy in the neutral O vacancies.

We now consider the thermodynamic stabilities of the oxygen vacancies at different temperatures and oxygen partial pressures. As shown in eqn (1), the formation energy of an oxygen vacancy is a function of the oxygen chemical potential, which is dependent on the experimental conditions such as temperature and pressure. The oxygen chemical potential is determined *via* eqn (2). The formation energy of an oxygen vacancy as a function of the Fermi energy and temperature are shown in Fig. 4, in which the oxygen partial pressure is fixed at 0.2 bar. Fig. 5 illustrates the formation energies of the charged O vacancies in bulk Li$_2$FeSiO$_4$ as a function of temperature when the Fermi levels are chosen to be at VBM ($\varepsilon_F = 0$) and CBM ($\varepsilon_F = E_g$), respectively, while the oxygen partial pressure is fixed to 0.2 bar. The results in Fig. 4 and 5 suggest that the O vacancy formation energy decreases with the increasing temperature for all three charged states, as expected. That is to say, as the temperature increases, the formation of oxygen vacancy becomes more favorable and the electrons occupied at the oxygen-vacancy-induced defect level can be more likely excited into the conduction bands, so that the oxygen vacancy is easily ionized. The thermodynamic transition level of V_O^{1+}/V_O^{2+} is

located just above the CBM, irrespective of the temperature and the oxygen partial pressure. The oxygen vacancy would act as an n-type dopant and introduce electron carriers in the Li$_2$FeSiO$_4$. Therefore, the V_O would increase the electronic conductivity of Li$_2$FeSiO$_4$.

The formation energies of the charged O vacancies as a function of the oxygen partial pressure at given temperatures of $T = 300$ K and $T = 1000$ K are shown in Fig. 6, when the Fermi levels are set to $\varepsilon_F = 0$ and $\varepsilon_F = E_g$, respectively. The vacancy formation energies increase with the increasing oxygen partial pressure, as expected. Contrary to the temperature, the enhanced pressure increased the formation energies of O vacancies. The negative and very small values of the O vacancy formation energies for V_O^{2+}, as shown in Fig. 6(a) and (b), suggest that the formations of V_O^{2+} are always energetically favorable over the entire range of pressure (from 10^{-10} to 10^{+3} atm) and at both the $T = 300$ K and $T = 1000$ K when the Fermi-level is at $\varepsilon_F = 0$. When the Fermi-level is at $\varepsilon_F = E_g$, all the formation energies of oxygen vacancies are fairly large for different charged states, over the entire range of pressure and at both $T = 300$ K and $T = 1000$ K, as shown in Fig. 6(c) and (d). The formation of V_O^{2+} is again more favorable than that of V_O^{1+} and V_O^0. Also, the higher temperature can enhance the effect of pressure on the O vacancy formation energies.

We now further discuss the effect of both the temperature and oxygen partial pressure on the formation energy of an O vacancy in *Pnma*-Li$_2$FeSiO$_4$, using neutral O vacancy as an example. The formation energy of an O vacancy, $E_f(O)$, given with respect to temperature and oxygen partial pressure, is shown in Fig. 7. Generally speaking, the $E_f(O)$ decreases with the increase of temperature and the decrease of oxygen partial pressure, as expected. That is, higher temperature and/or lower oxygen partial pressure would easily lead to the formation of the oxygen vacancy. A black arrow in Fig. 7, as a guide to the eyes, shows the fastest decreasing direction of the vacancy formation energy. Thus, to govern the appearance of oxygen vacancies, one can decrease or enhance the temperature and/or the pressure during the preparation of the material.

After the discussion on the formation of a single oxygen vacancy, we proceed with the discussion on the change of electronic structures due to the introduction of an oxygen vacancy. We first calculate the deformation charge densities in both the perfect and defected Li$_2$FeSiO$_4$ (*i.e.*, without and with oxygen vacancy), which are shown in Fig. 8(a) and (b), respectively. The deformation charge density here is defined as the difference between the total charge density $\rho(\vec{r})$ and the superposition of independent atomic charge density in the same system, that is

$$\Delta\rho(\vec{r}) = \rho(\vec{r}) - \sum_\mu \rho_{atom}(\vec{r} - \vec{R}_\mu) \tag{3}$$

where $\vec{R}_\mu$ are the atomic positions. The solid and dashed lines in Fig. 8 represent the accumulation and depletion of charges relative to the independent atoms, respectively. Such a deformation charge density can help visualize the bonding characters in a material. Fig. 8(a) and (b) indicate that the bonding character in *Pnma*-Li$_2$FeSiO$_4$ is clearly covalent mixed with ionic. The comparison
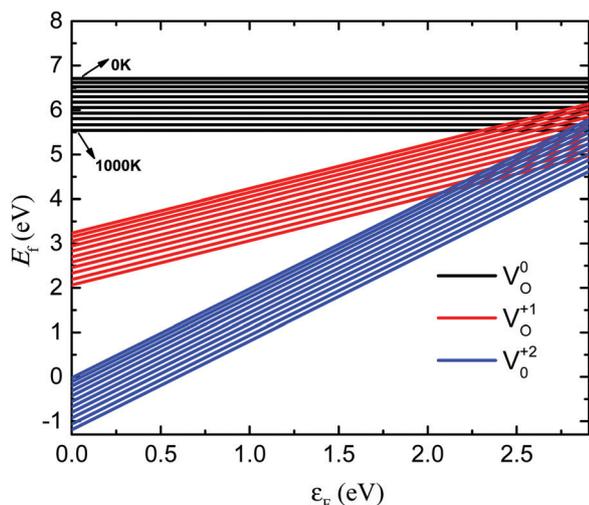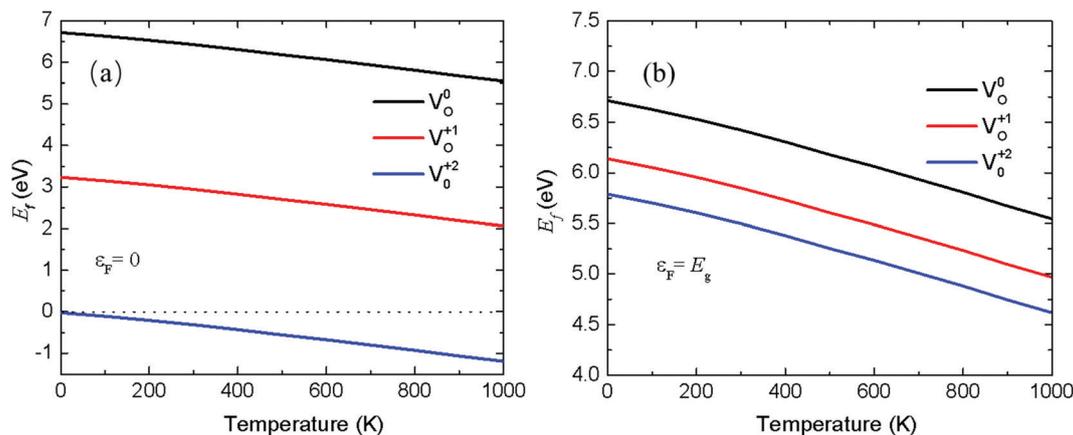

Fig. 4 Formation energies of O vacancies as a function of Fermi energy at different charge states, with a 0.2 bar oxygen gas phase, corresponding to a series of temperatures with an increment of 100 K.

This journal is © the Owner Societies 2021

Phys. Chem. Chem. Phys., 2021, **23**, 20444–20452 | **20447**

Fig. 5 Formation energies of O vacancies at different charged states as a function of temperature in *Pnma*-Li$_2$FeSiO$_4$, at 0.2 bar oxygen partial pressure and $\varepsilon_F = 0$ and $\varepsilon_F = E_g$, respectively.
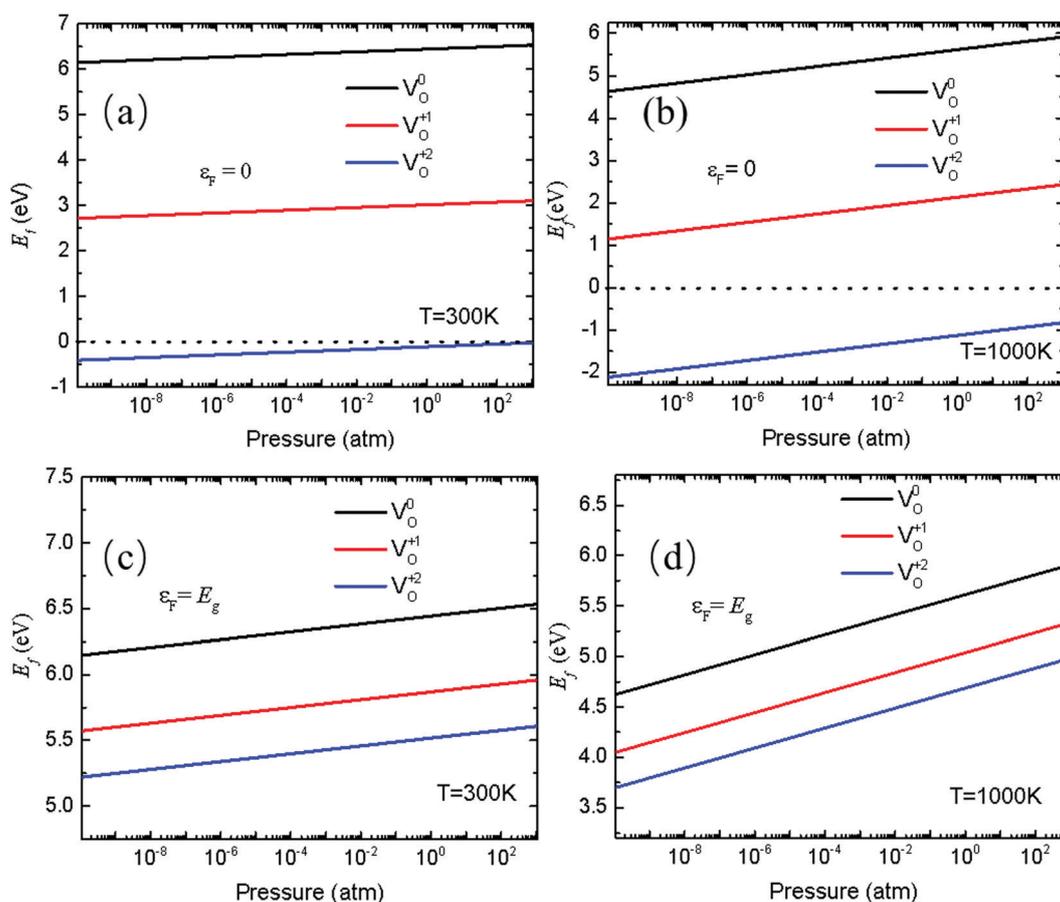

Fig. 6 Formation energies of O vacancies at different charge states as a function of the oxygen partial pressure at given temperatures of $T = 300$ K and $T = 1000$ K, and (a) and (b) for $\varepsilon_F = 0$ and (c) and (d) $\varepsilon_F = E_g$, respectively.

between Fig. 8(a) and (b) shows that only the charge densities around Fe in the vicinity of the oxygen vacancy are somewhat distorted, while a minor charge redistribution occurs only around the Si sites in the vicinity of the oxygen vacancy. Such a picture indicates that the influence of the oxygen vacancy in the host material is very localized. This localization is due to the insulating character of Li$_2$FeSiO$_4$ where all bonds in the material are saturated. This is very different from the Al-vacancy in metal aluminum, where the influence of the vacancy in the host material Al is very much extended.[46]
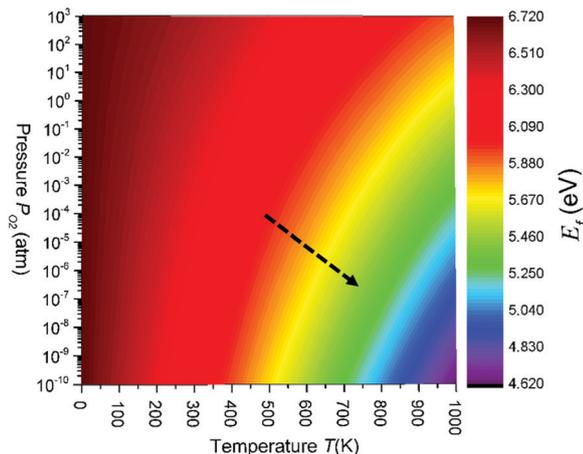
20448 | *Phys. Chem. Chem. Phys.*, 2021, **23**, 20444–20452

This journal is © the Owner Societies 2021

Fig. 7 Calculated formation energies for the neutral O vacancies as a function of temperature T and oxygen partial pressure P. As a guide to the eyes, the black dotted arrow points to the fastest decreasing direction of the vacancy formation energy.
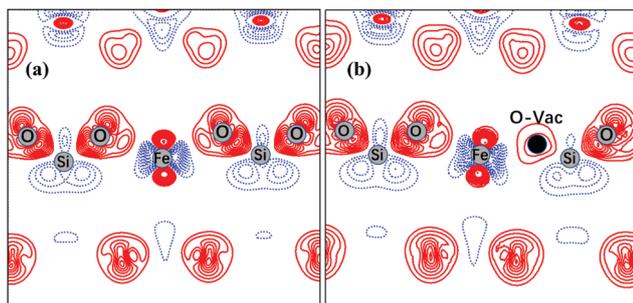

Fig. 8 Deformation charge densities for the supercell (a) without and (b) with an oxygen vacancy. The black dot in (b) represents the position of the oxygen vacancy.

Since the influence on the host material arising from the oxygen vacancy is very localized, we show in Fig. 9 the partial densities of states (PDOS) of only the Fe and Si ions in the vicinity of the vacancy, for further understanding the oxygen-vacancy-induced defect states in $Pnma$-Li$_2$FeSiO$_4$. Based on the above analysis on the charge density redistributions, only the PDOS of the Fe and Si ions in the vicinity of the vacancy are depicted in Fig. 9(a). As seen in Fig. 9(a) and (d), the defect levels induced by the neutral oxygen vacancy appear just above the VBM and are fully occupied. The corresponding electronic states are contributed mainly by the nearby Fe and Si atom next to the vacancy site. For the V_O^{1+}, its defect levels are partially occupied and exhibit a large spin-splitting. For the V_O^{2+}, the corresponding defect states appear just below the CBM and become fully unoccupied.

3.2 Influence of cation defects on the formation of an oxygen vacancy

To study the influence of doping/defect on the formation of an oxygen vacancy, herein we consider the effects of two types of defects. One type is the Mn and Co substitution for the Fe site

(denoted as Mn$_{Fe}$ and Co$_{Fe}$), the other contains the Fe-vacancy and two Li-vacancies (denoted as V_{Fe} and V_{2Li}). Only those substitutional and vacancy defects in the vicinity of the O-vacancy are considered. The interaction energy E_{int} between a substitutional defect and a V_O are calculated by the expression:[47]

$$
\begin{aligned}
E_{int} &= [E(X_{Fe} + V_O) + E_0] - [E(X_{Fe}) + E(V_O)] \\
&= E_f(X_{Fe} + V_O) - E_f(X_{Fe}) - E_f(V_O) \quad (X = Mn, Co)
\end{aligned}
$$
(4)

where $E(X_{Fe} + V_O)$, $E(X_{Fe})$ and $E(V_O)$ are the total energies of the supercells with a complex defect of $X_{Fe} + V_O$, a single X_{Fe}, and a single V_O, respectively, which are all calculated in the same supercell but with different defects. The negative value of E_{int} represents the attraction between a X_{Fe} and a V_O, while the positive value of E_{int} implies the repulsion between the defects.

The calculated interaction energies between substitutional defects (*i.e.*, Mn$_{Fe}$ and Co$_{Fe}$) and oxygen vacancy are presented in Fig. 10. We can see that the interaction energies between substitutional defects and the neighboring oxygen vacancy are small (*i.e.*, in the range of −0.4 to −0.2 eV). This is because Mn^{2+}, Co^{2+} and Fe^{2+} are chemically rather similar. The negative values of the interaction energies, although they are small, indicate the attraction between substitutional defects and the oxygen vacancies. In fact, E_{int} can be viewed as the change in formation energy of V_O caused by the above types of defects, which is also the change in the formation energies of the defects caused by V_O. The negative E_{int} (*i.e.*, the attraction) suggests that the formation energy of an oxygen vacancy is reduced once the substitutional defect is introduced. These results suggest that the substitutional Co defect would be more likely to boost the formation of an oxygen vacancy than the substitutional Mn defect.

For the interaction energies E_{int} between the cation vacancy defects (*i.e.*, V_{2Li} and V_{Fe}) and the oxygen vacancy, they are calculated as

$$
\begin{aligned}
E_{int} &= [E(V_X + V_O) + E_0] - [E(V_X) + E(V_O)] \\
&= E_f(V_X + V_O) - E_f(V_X) - E_f(V_O) \\
&(X = 2Li, Fe)
\end{aligned}
$$
(5)

The corresponding E_{int} is also presented in Fig. 10. We can see that the attractive interactions between the cation vacancy defects (*i.e.*, V_{2Li} and V_{Fe}) and the oxygen vacancy are quite strong, as compared to the substitutional defects mentioned above. The interaction energy between V_{Fe} and V_O is quite significant (−4.79 eV), indicating that the formation of an oxygen vacancy becomes much easier when V_{Fe} is created in the vicinity of an oxygen vacancy. The formation energy of an O vacancy would be reduced by 1.38 eV when two lithium vacancies (V_{2Li}) are introduced around the oxygen vacancy. To maintain the charge compensation as much as possible, the formation of a cation vacancy may be accompanied by the formation of an oxygen vacancy.
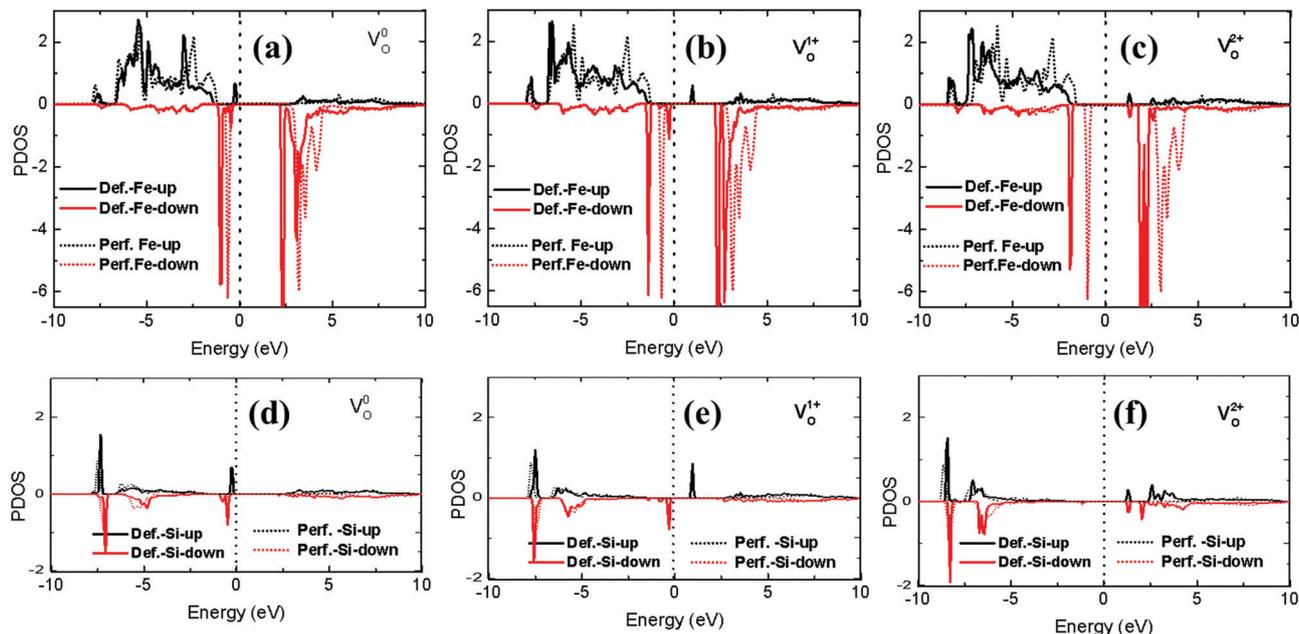
Fig. 9 Calculated partial density of states (PDOS) of the Fe and Si ions in the vicinity of the O vacancy with different charge states, compared with those of perfect Li_2FeSiO_4. (a)−(c) are for Fe ions and (d)−(f) for Si ions. Dotted and solid lines correspond to PDOSs in the perfect and defected supercell, respectively.
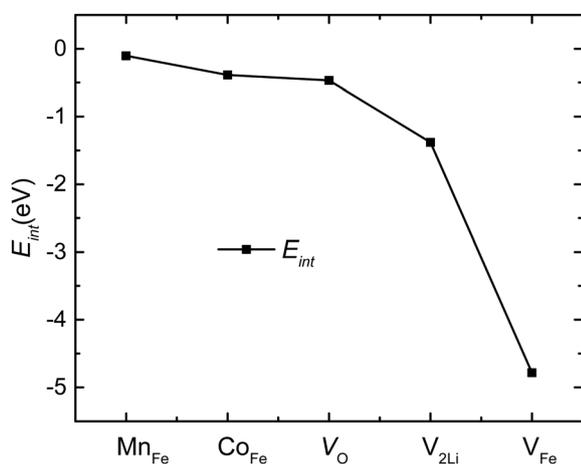

Fig. 10 Interaction energy E_{int} between Mn_{Fe}, Co_{Fe}, V_O, V_{2Li}, V_{Fe} and a single V_O, respectively.

3.3 Influence of O vacancy concentration on the formation energy of an O vacancy

Finally, we studied the double oxygen vacancies (V_{2O}) to check the dependence of the formation energy of an oxygen vacancy on the concentration of oxygen. The double oxygen vacancies were considered by the removal of two nearest-neighboring oxygen atoms from the $2 \times 2 \times 2$ supercell of Li_2FeSiO_4, corresponding to an oxygen vacancy concentration of 1.5%. We have calculated the formation energies of V_{2O} with different charged states ($q = 0, +1, +2, +3$ and $+4$) and made a comparison with the formation energies of a single oxygen vacancy, discussed in the previous sections. Firstly, the interaction energy

between two neutral oxygen vacancies is also shown in Fig. 10 and the corresponding value is about -0.47 eV, which suggests that the oxygen vacancies would be energetically aggregated. Secondly, the formation energy of V_{2O}^{2+} is about -0.28 eV smaller than the sum of the formation energies of two isolated V_O^{1+}s. Similarly, the formation energies of V_{2O}^{3+} is about -1.90 eV smaller than the sum of the formation energies of an isolated V_O^{2+} and a V_O^{1+}, while the formation energies of V_{2O}^{4+} is about -2.01 eV smaller than the sum of the formation energies of two isolated V_O^{2+}. The above comparison indicates that the double oxygen vacancies also prefer the fully ionized charge state, just like the single oxygen vacancy.

4. Conclusion

In conclusion, we have employed first-principles calculations to study the formation energies of oxygen vacancies with their relevant charge states in the bulk $Pnma$-Li_2FeSiO_4. The formation energy of the V_O plays a crucial role in determining the possible occurrence of the V_O. The formation energies of a V_O are essentially dependent on the experimental conditions. As expected, the increased temperature, decreased oxygen partial pressure and Fermi level decrease the formation energy of the oxygen vacancy. The calculated formation energies of oxygen vacancies in different charge states indicate that the oxygen vacancy in Li_2FeSiO_4 would be energetically favorable to be fully ionized. We found that the presence of V_O was accompanied by a distinct redistribution of the electronic charge densities only around the Fe and Si ions in the vicinity of the O-vacancy, which shows a very local influence on the host material arising from V_O. Such a local characteristic is also confirmed by the

20450 | *Phys. Chem. Chem. Phys.*, 2021, **23**, 20444–20452

This journal is © the Owner Societies 2021

calculated electronic partial densities of states (PDOS). We have also discussed the influences of the substitutional defects (Mn_{Fe}, Co_{Fe}) on the formation of V_O and the vacancies (V_{Fe}, V_{2Li}) in the vicinity of the O-vacancy, respectively. We found that the interaction energies between V_O and these two types of defects are all negative, indicating that the generation of an O-vacancy becomes more favorable by introducing the above defects. The substitutional defects (Mn_{Fe} and Co_{Fe}) cause only small influences on the formation of V_O while the vacancy defects (V_{Fe}, V_{2Li}) have large influences on the formation of V_O. In addition, the attractive interaction between two oxygen vacancies indicates that the oxygen vacancies in Li_2FeSiO_4 would be aggregated. The double oxygen vacancies in Li_2FeSiO_4 also prefer the fully ionized charge states. Our calculations can help understand the formation of oxygen vacancies in Li_2FeSiO_4, and provide guidelines for the anion defect engineering to help develop the cathode materials for the high-performance lithium-ion batteries.

Conflicts of interest

There are no conflicts to declare.

Acknowledgements

References

1 C. Y. Ouyang and L. Chen, *Sci. China: Phys., Mech. Astron.*, 2013, **56**, 2278–2292.

2 M. S. Whittingham, *Chem. Rev.*, 2004, **104**, 4271–4301.

3 D. Jiang, Y. Jiang, Z. Li, T. Liu, X. Wo, Y. Fang, N. Tao, W. Wang and H.-Y. Chen, *J. Am. Chem. Soc.*, 2017, **139**, 186–192.

4 M. Hirooka, T. Sekiya, Y. Omomo, M. Yamada, H. Katayama, T. Okumura, Y. Yamada and K. Ariyoshi, *J. Power Sources*, 2020, **463**, 228127.

5 Q. Li, J. Zhang, C. Gong, J. Guo, L. Yu and J. Zhang, *Ceram. Int.*, 2019, **45**, 13198–13202.

6 D. Santos-Carballal, P. E. Ngoepe and N. H. de Leeuw, *Phys. Rev. B*, 2018, **97**, 085126.

7 A. K. Padhi, K. S. Nanjundaswamy and J. B. Goodenough, *J. Electrochem. Soc.*, 1997, **144**, 1188–1194.

8 C. Sun, S. Rajasekhara, J. B. Goodenough and F. Zhou, *J. Am. Chem. Soc.*, 2011, **133**, 2132–2135.

9 A. Nytén, A. Abouimrane, M. Armand, T. Gustafsson and J. O. Thomas, *Electrochem. Commun.*, 2005, **7**, 156–160.

10 M. E. Arroyo-de Dompablo, M. Armand, J. M. Tarascon and U. Amador, *Electrochem. Commun.*, 2006, **8**, 1292–1298.

11 D. Li, R. Xie, M. Tian, S. Ma, L. Gou, X. Fan, Y. Shi, H.-T.-H. Yong and L. Hao, *J. Mater. Chem. A*, 2014, **2**, 4375–4383.

12 D. Lv, W. Wen, X. Huang, J. Bai, J. Mi, S. Wu and Y. Yang, *J. Mater. Chem.*, 2011, **21**, 9506–9512.

13 R. Dominko, M. Bele, M. Gaberšček, A. Meden, M. Remškar and J. Jamnik, *Electrochem. Commun.*, 2006, **8**, 217–222.

14 J. Moskon, R. Dominko, R. Cerc-Korosec, M. Gaberscek and J. Jamnik, *J. Power Sources*, 2007, **174**, 683–688.

15 Y. Fujita, T. Hira, K. Shida, M. Tsushida, J. Liao and M. Matsuda, *Ceram. Int.*, 2018, **44**, 11211–11217.

16 Z. Zheng, Y. Wang, A. Zhang, T. Zhang, F. Cheng, Z. Tao and J. Chen, *J. Power Sources*, 2012, **198**, 229–235.

17 P. Vajeeston, *Mater. Lett.*, 2018, **218**, 313–316.

18 S. Chakrabarti, A. K. Thakur and K. Biswas, *Electrochim. Acta*, 2017, **236**, 288–296.

19 R. Dominko, *J. Power Sources*, 2008, **184**, 462–468.

20 S. Zhang, C. Deng, B. L. Fu, S. Y. Yang and L. Ma, *Electrochim. Acta*, 2010, **55**, 8482–8489.

21 C. Deng, S. Zhang, S. Y. Yang, B. L. Fu and L. Ma, *J. Power Sources*, 2011, **196**, 386–392.

22 L. Qu, D. Luo, S. Fang, Y. Liu, L. Yang, S.-I. Hirano and C.-C. Yang, *J. Power Sources*, 2016, **307**, 69–76.

23 W. Sukkabot, *Mater. Chem. Phys.*, 2019, **229**, 467–473.

24 M. Bini, S. Ferrari, C. Ferrara, M. C. Mozzati, D. Capsoni, A. J. Pell, G. Pintacuda, P. Canton and P. Mustarelli, *Sci. Rep.*, 2013, **3**, 3452.

25 T. Nakamura, K. Ohta, X. Hou, Y. Kimura, K. Tsuruta, Y. Tamenori, R. Aso, H. Yoshida and K. Amezawa, *J. Mater. Chem. A*, 2021, **9**, 3657–3667.

26 P. Xiao, Z. Q. Deng, A. Manthiram and G. Henkelman, *J. Phys. Chem. C*, 2012, **116**, 23201–23204.

27 W. Hu, H. Wang, W. Luo, B. Xu and C. Ouyang, *Solid State Ionics*, 2020, **347**, 115257.

28 R. Huang, Y. H. Ikuhara, T. Mizoguchi, S. D. Findlay, A. Kuwabara, C. A. Fisher, H. Moriwake, H. Oki, T. Hirayama and Y. Ikuhara, *Angew. Chem., Int. Ed.*, 2011, **50**, 3053–3057.

29 P. Zhang and S.-H. Wei, *Electrochim. Acta*, 2018, **270**, 409–416.

30 F. Zheng, S. Zheng, P. Zhang, X. Zhang, S. Wu, Y. Yang and Z. Z. Zhu, *J. Phys. Chem. C*, 2019, **123**, 13491–13499.

31 R. A. House, U. Maitra, L. Jin, J. G. Lozano, J. W. Somerville, N. H. Rees, A. J. Naylor, L. C. Duda, F. Massel, A. V. Chadwick, S. Ramos, D. M. Pickup, D. E. McNally, X. Lu, T. Schmitt, M. R. Roberts and P. G. Bruce, *Chem. Mater.*, 2019, **31**, 3293–3300.

32 G. Kresse and J. Furthmuller, *Phys. Rev. B: Condens. Matter-Mater. Phys.*, 1996, **54**, 11169–11186.

33 G. Kresse and J. Furthmuller, *Comput. Mater. Sci.*, 1996, **6**, 15–50.

34 P. E. Blöchl, *Phys. Rev. B: Condens. Matter Mater. Phys.*, 1994, **50**, 17953.

35 J. P. Perdew, K. Burke and M. Ernzerhof, *Phys. Rev. Lett.*, 1996, **77**, 3865–3868.

36 H. J. Monkhorst and J. D. Pack, *Phys. Rev. B: Solid State*, 1976, **13**, 5188–5192.

37 S. L. Dudarev, G. A. Botton, S. Y. Savrasov, C. J. Humphreys and A. P. Sutton, *Phys. Rev. B: Condens. Matter Mater. Phys.*, 1998, **57**, 1505–1509.

38 S. B. Zhang and J. E. Northrup, *Phys. Rev. Lett.*, 1991, **67**, 2339–2342.

39 C. G. Van de Walle and J. Neugebauer, *J. Appl. Phys.*, 2004, **95**, 3851–3879.

This journal is © the Owner Societies 2021

Phys. Chem. Chem. Phys., 2021, **23**, 20444–20452 | **20451**

40 Y. Kumagai and F. Oba, *Phys. Rev. B: Condens. Matter Mater. Phys.*, 2014, **89**, 195205.

41 C. Y. Ouyang, Ž. Šljivančanin and A. Baldereschi, *Phys. Rev. B: Condens. Matter Mater. Phys.*, 2009, **79**, 235410.

42 L. Wang, T. Maxisch and G. Ceder, *Phys. Rev. B: Condens. Matter Mater. Phys.*, 2006, **73**, 195107.

43 K. Reuter and M. Scheffler, *Phys. Rev. B: Condens. Matter Mater. Phys.*, 2001, **65**, 035406.

44 X. Zhao, S. Wu, X. Lv, M. C. Nguyen, C. Z. Wang, Z. Lin, Z. Z. Zhu and K. M. Ho, *Sci. Rep.*, 2015, **5**, 15555.

45 F. Zheng, Q. Lin, S. Wu and Z. Z. Zhu, *Solid State Ionics*, 2020, **356**, 115436.

46 D. E. Turner, Z. Z. Zhu, C. T. Chan and K. M. Ho, *Phys. Rev. B: Condens. Matter Mater. Phys.*, 1997, **55**, 13842–13852.

47 W. Zhang and Z. F. Hou, *J. Appl. Phys.*, 2014, **115** 124104.